Cellulose (2024) 31:8189–8202
https://doi.org/10.1007/s10570-024-06077-3

ORIGINAL RESEARCH

Xanthan/ carboxymethyl cellulose-based edible coatings enriched with greenly synthesized ZnO-NPs for active packaging applications

Hend E. Salama · Maher A. Khattab · Magdy W. Sabaa · Mohamed S. Abdel Aziz

Received: 24 May 2023 / Accepted: 19 July 2024 / Published online: 9 August 2024
© The Author(s) 2024

Abstract The limited use of xanthan (Xa) and carboxymethyl cellulose (CMC) in the food packaging industry is due to their poor barrier and antimicrobial properties. The objective of this work was to enhance the characteristics of the CMC/Xa composite coating by incorporating ZnO nanoparticles (ZnO-NPs) that were prepared through a green method through *Coriandrum sativum* extract. FTIR and XRD confirmed the successful preparation of the coating and verified the interactions between its components. Compared to the neat CMC/Xa system, systems incorporated with ZnO-NPs exhibited excellent water barrier, mechanical, thermal, and antimicrobial characteristics. The CMC/Xa/ZnO-NP systems effectively prolonged the shelf life of tomatoes for a storage period of 20 days without any significant indications of spoilage or mass loss of the coated tomatoes. The obtained results indicated that the developed coating has the potential to replace traditional plastic packaging and effectively preserve food products.

Keywords Edible coating · Carboxymethyl cellulose · Xanthan; ZnO-NPs · Active packaging

Introduction

Edible coatings are a promising solution for extending the shelf life of food and enhancing its quality by creating a protective layer on the food surface. Edible coatings made from biodegradable polymers have gained significant attention because of their biocompatibility, biodegradability, and edibility (Abdel Aziz et al. 2021). Biodegradable polymers have numerous functional groups that can be easily modified to other derivatives of improved properties. These derivatives might be suitable replacements for the non-degradable plastics used in food packaging (Abdel Aziz et al. 2018).

Carboxymethyl cellulose (CMC), a water-soluble cellulose derivative, is a common base material for producing edible coatings. It is a non-toxic, transparent, and biodegradable polymer. Moreover, CMC could form elastic films (Salama et al. 2020). However, its application in food packaging is limited by several factors, such as poor inhibition of food-spoiling pathogens (Azhdari et al. 2022). Additionally, CMC films exhibit insufficient water barrier properties owing to their hydrophilic nature, as well as their inadequate UV-shielding abilities (Salama et al. 2020).

Supplementary Information The online version contains supplementary material available at https://doi.org/10.1007/s10570-024-06077-3.

H. E. Salama (✉) · M. A. Khattab · M. W. Sabaa · M. S. A. Aziz
Chemistry Department, Faculty of Science, Cairo University, Giza 12613, Egypt
e-mail: hendezzat2010@cu.edu.eg; hezzat@sci.cu.edu.eg

Xanthan (Xa) is a noteworthy anionic polysaccharide that is produced by the bacteria *Xanthomonas campestris* and is readily soluble in water (Xu et al. 2018). The side chains of Xa contain both glucuronic acid and pyruvic acid groups, which contribute to its anionic characteristics (Xu et al. 2018). Owing to its biocompatibility, biodegradability, thermal stability, and non-toxicity, Xa has extensive applications in various industries such as biomedicals (Petri 2015), food (Ostrowski et al. 2022), pharmaceuticals (Banerjee et al. 2019), and cosmetics (Chaturvedi et al. 2021). Xa contains numerous hydroxyl groups and free carboxyl groups, which make it ideal for chemical modifications and/or functionalization to optimize its physicochemical properties. Xa can form physical networks with other several polysaccharides, including galactomannans (Hayta et al. 2020), guar gum (Ren et al. 2022), konjac glucomannan (Yang et al. 2020), and chitosan (Ćirić et al. 2021). These networks can be established through different mechanisms such as hydrogen bonding, hydrophobic interactions, and cation bridging. The Food and Drug Administration (FDA) has approved Xa as a safe polymer for use in the food industry (Joshy et al. 2020). Owing to its high acid/salt resistance and high pseudo-plasticity, Xa is widely utilized in the food industry as a thickener agent (Nsengiyumva et al. 2022). The viability of Xa for use in food packaging is constrained by various limitations, including inadequate antimicrobial inhibition, poor barrier properties, and limited solubility (Fan et al. 2021).

The incorporation of diverse additives, such as nanomaterials, is beneficial for enhancing the effectiveness of edible coatings (Smaoui et al. 2023). Among these outstanding nanomaterials, ZnO-NPs have been safely included in various food coatings owing to their outstanding antimicrobial and biocompatibility properties. ZnO-NPs have been approved by the FDA as safe for human consumption (Priyadarshi et al. 2017). In addition to improving the mechanical, thermal, and barrier properties of edible coatings, the incorporation of ZnO-NPs can significantly improve their UV-shielding properties (Abdel Aziz et al. 2022). ZnO-NPs have been successfully incorporated into various coating systems, including carrageenan (Praseptiangga et al. 2021), chitosan (Noshirvani et al. 2017), and carboxymethyl cellulose (Li et al. 2021), resulting in considerable improvements. Typically, ZnO-NPs are produced by reducing zinc salts, such as zinc nitrate or zinc acetate (Abdel Aziz et al. 2022). However, the use of plant extracts for the preparation of ZnO-NPs is gaining popularity as an eco-friendly method that produces nanoparticles with potent antioxidant and antimicrobial properties (Surendra et al. 2022).

This study involved the use of a green method to prepare ZnO-NPs, which were then added to a composite system consisting of CMC and Xa. The resulting edible system was created to have customized properties suitable for food packaging. The physical and antimicrobial properties of the coatings were also investigated. A preliminary study was carried out to assess the packaging efficiency of the coating in prolonging the shelf life of tomatoes.

Experimental

Materials

CMC ($M_n = 9 \times 10^4$ g mol^{-1}, $DS = 0.75$) was supplied from Acros Organics (USA). Xanthan was provided from Alpha-Chemika (India, $M_n = 1.7 \times 10^6$ g mol^{-1}). Glycerol, calcium chloride, sodium hydroxide, zinc acetate, and all solvents were supplied from Sigma-Aldrich (Germany). *Coriandrum sativum* was obtained from the local market (Egypt).

Preparation of ZnO-NPs

The green approach by Naseer et al. (2020) was utilized to obtain ZnO-NPs using *Coriandrum sativum* (CS) extract. Initially, the leaves of CS were washed with distilled water to eliminate impurities. After drying, 5 g of the leaves were mixed with 200 mL of distilled water and heated at 70 °C for 30 min. The mixture was then filtered and stored at 4 °C. Zinc acetate (0.01 M) was added to the extract and the pH was adjusted to 12 using 1.0 M NaOH. The reaction mixture was continuously stirred at 70 °C for 2 h, resulting in a pale-white precipitate of ZnO-NPs. The obtained ZnO-NPs were rinsed multiple times with deionized water to eliminate impurities and excess NaOH. Subsequently, the ZnO-NPs were dried overnight under a vacuum at 60 °C. Scheme 1 outlines the green preparation pathway of ZnO-NPs.



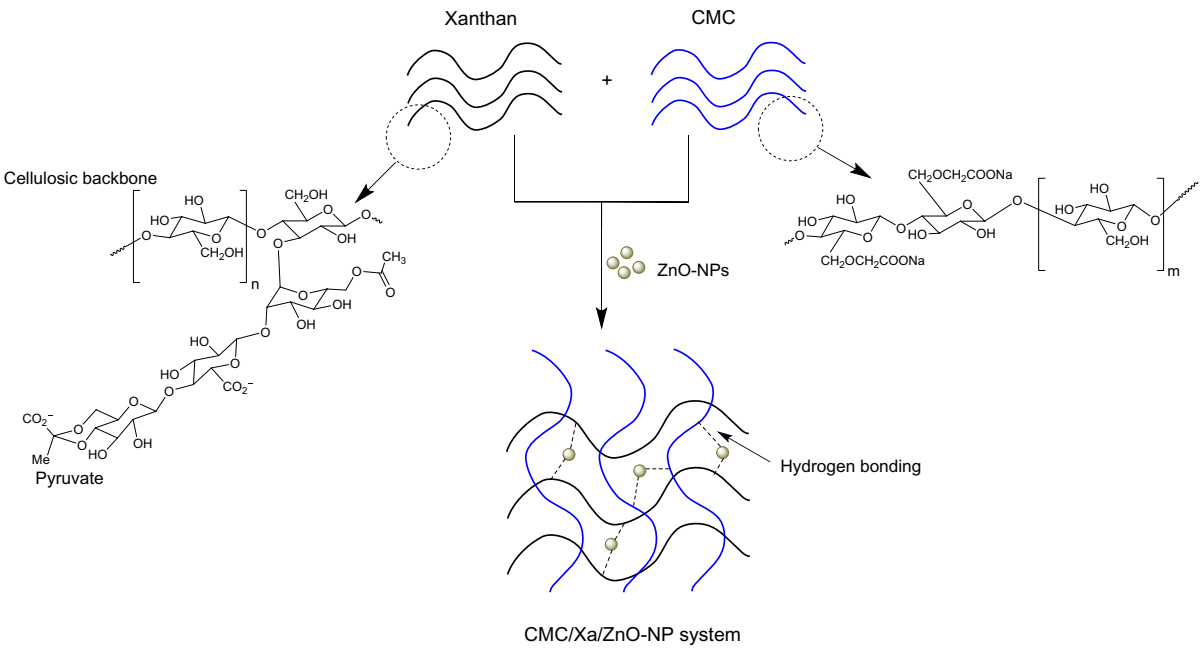
Scheme 1 Green preparation of ZnO-NPs through CS extract

Preparation of CMC/Xa and CMC/Xa/ZnO-NP films

Initially, CMC (1 g) and Xa (1 g) were individually dissolved in distilled water (50 mL), mixed, and stirred until homogeneity was achieved. Next, glycerol (plasticizer) was added at 40 wt% to the reaction mixture and stirred for 2 h at room temperature. ZnO-NPs were added at different percentages of 0, 3 and 5 wt% (based on the total mass of CMC and Xa) to the prepared CMC/Xa mixtures. The resulting solution mixture was poured into a 10 cm Petri dish and then dried for 24 h at 40 °C in a vacuum oven. The dried films were immersed in 45 mL of 1% $CaCl_2$ (crosslinking agent) for 2 h in an oven at 40 °C. Finally, the films were removed from the Petri dishes, rinsed with distilled water, and dried in a vacuum oven. The systems were coded according to the format CMC/Xa/*y*ZnO, where *y* represents the weight percentage of ZnO-NPs present in each system. A sample without ZnO-NPs (CMC/Xa) was employed as a control to investigate the impact of ZnO-NPs. The preparation process is shown in Scheme 2.

Shelf-life studies

Fresh tomatoes (*Solanum lycopersicum L*) of comparable size and free of defects were used in the shelf-life studies. First, the tomatoes were disinfected for two minutes with a 0.1 g/L hypochlorite solution, washed with distilled water, and dried at room



Scheme 2 Preparation of CMC/Xa/ZnO-NP coating system

temperature. The dipping method was then used to apply a thin coating to the surface of the tomatoes using a mixture of CMC, Xa, and ZnO-NPs from the CMC/Xa/3ZnO system (prepared according to the aforementioned method). Another coating mixture without ZnO-NPs (CMC/Xa) was also prepared for comparison. To form a crosslinked coating layer on the tomato surface, the coated tomatoes were dipped in a $CaCl_2$ solution (1%) for one minute and then air-dried before being dipped again. The mass loss of the coated and uncoated tomatoes during storage was determined by measuring the mass of the tomatoes every two days. The percentage of mass loss was calculated using Equation 1:

$$\text{Mass loss } (\%) = \frac{m_o - m_t}{m_o} \times 100 \tag{1}$$

where m_t and m_o represent the mass (gram) of tomatoes after a certain storage interval, and that on the first day, respectively. Measurements were performed in triplicate for three tomatoes of comparable size, and the results were averaged. Surface spoilage of the tomatoes was visually monitored during storage periodically by capturing images of their surfaces.

Characterization techniques

The KBr dry method was utilized to conduct FTIR analysis using a Perkin-Elmer B25 spectrophotometer (USA). The samples were dried and scanned in the 4000–400 cm^{-1} region with a resolution of 4 cm^{-1} and an average of 15 scans.

The mechanical properties of films were evaluated utilizing the Zwick 1445 following ASTM D882-2010 (International 2012). For each film, the mean value was recorded based on five repeated tests. Further information regarding the measurement procedure was provided in the Supplementary Information S1.

The ability of the film to act as a water barrier was evaluated by calculating the water vapor permeability according to ASTM E96-92 (1990) (ASTM). The measurement procedure described in the Supplementary Information S1 was used to obtain the average value of three separate measurements for each sample.

Philips Xpert MPD Pro (Netherlands) was used to study XRD patterns at room temperature. Cu-Kα_1 radiation (λ = 1.54056 Å) was utilized to analyze each film over the 2θ range of 5°–80° with a scanning rate of 1°min^{-1}. OriginPro software was used to adjust the baseline and decrease noise in the XRD curves. Three models were utilized to determine the average crystallite size (D) of the prepared ZnO-NPs based on their XRD pattern:

Scherrer model:

$$\cos\theta = \frac{k\lambda}{D}\left(\frac{1}{\beta}\right) \tag{2}$$

where k is the Scherrer constant (0.9), λ is the radiation wavelength, and β and θ are the full width at half maximum and Bragg angle of the diffraction peaks, respectively. Plots were generated with $1/\beta$ on the X-axis and $\cos\theta$ on the Y-axis, representing different diffraction peaks. By data fitting, the crystallite size (D) was extracted from the slope of the fitted line using the formula $D = k\lambda$/slope.

Williamson-Hall (W-H):

$$\beta\cos\theta = \frac{k\lambda}{D} + 4\varepsilon\sin\theta \tag{3}$$

where ε is the lattice strain. The value of D was determined from the intercept of the fitted line of a plot representing $4\sin\theta$ on the X-axis and $\beta\cos\theta$ on the Y-axis, utilizing the formula $D = k\lambda$/intercept.

Halder-Wagner (H-W) (Sen et al. 2020)*:*

$$\left(\frac{\beta^*}{d^*}\right)^2 = \frac{\beta^*}{d^{*2}}\left(\frac{1}{D}\right) + \frac{\varepsilon^2}{4} \tag{4}$$

where

$$\beta^* = \frac{\beta\cos\theta}{\lambda} \tag{5}$$

$$d^* = \frac{2\sin\theta}{\lambda} \tag{6}$$

D was calculated from a plot of $\left(\frac{\beta^*}{d^*}\right)^2$ versus $\frac{\beta^*}{d^{*2}}$, after linear regression, where D = 1/slope.

The JEOL transmission electron microscope (JEM-1400 TEM) with an acceleration voltage of 100 kV was used to capture TEM images of the prepared ZnO-NPs. Before imaging, ZnO-NPs were sonicated in water for an hour. A drop of the

obtained ZnO-NPs suspension was placed on carbon-coated copper grids. The size distribution of the ZnO-NPs was determined using ImageJ software (version 1.53t).

The Malvern Zeta potential analyzer (UK) was used to measure the hydrodynamic size of sonicated ZnO-NPs suspension in distilled water.

The Shimadzu TGA-50 H Thermal Analyzer (Japan) was utilized to assess the thermal properties. The analysis involved subjecting the samples (approximately 5 mg) to a nitrogen atmosphere at a rate of 10 °C min^{-1} within the temperature range of 20–600 °C. Thermal stability was evaluated by determining the integral procedure decomposition temperature (IPDT) (Doyle 1961). The IPDT was obtained from the TGA thermograms and was calculated as follows:

$$IPDT = A.K\left(T_f - T_i\right) + T_i \tag{7}$$

The terms A, K, T_f, and T_i were determined by analyzing the TGA curves, which can be found in the Supplementary Information S2.

The microbial inhibition of the coatings was evaluated using the agar well diffusion method (Miles et al. 1996). The used representative microorganisms were *Bacillus subtilis* (Gram-positive bacteria), *Escherichia coli* (Gram-negative bacteria), and *Syncephalastrum racemosum* (Fungi). The diameter of the inhibition zone (mm) was measured to determine the level of microbial inhibition. Measurements were obtained from three replicates and averaged.

The opacity of the films was measured by using the Shimadzu UV-VIS 3101-PC spectrophotometer, as follows:

$$\text{Opacity} = \frac{A_{600}}{m} \tag{8}$$

where A_{600} represents the absorbance of the films at 600 nm, and m denotes the film thickness (mm). Three measurements were recorded for each film to ensure precision.

Statistical analysis of variance (ANOVA) of repeated measurements was conducted using OriginPro software (Version 2022). The mean ± standard deviation for the repeated measurements was determined, and the variance between the samples was evaluated using the Tukey test with a significance level set at $p \leq 0.05$.

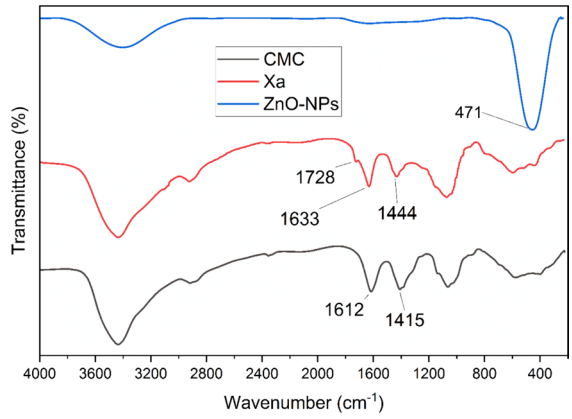


Fig. 1 FTIR spectra of ZnO-NPs, CMC, and Xa films

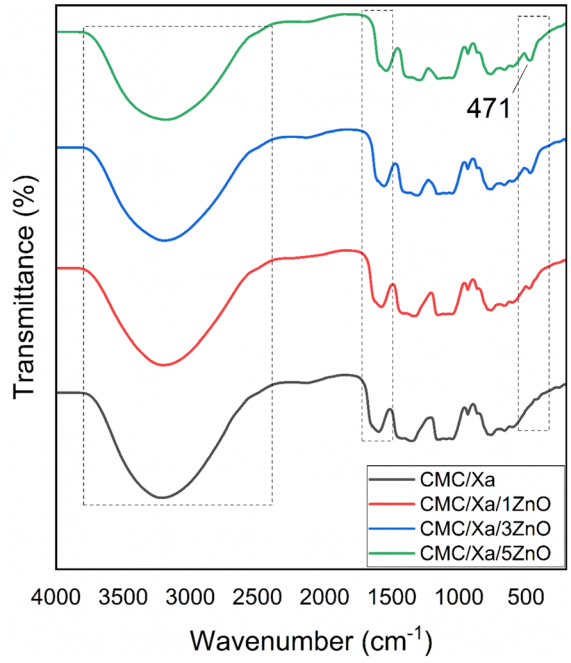


Fig. 2 FTIR spectra of CMC/Xa and CMC/Xa/ZnO-NP systems

Results and discussion

FTIR

The FTIR spectra of ZnO-NPs, CMC, and Xa are shown in Fig. 1, whereas Fig. 2 shows the spectra of CMC/Xa and CMC/Xa/ZnO-NP systems.

The spectrum of ZnO-NPs exhibited a broad band at approximately 3415 cm^{-1}, which was assigned to the stretching vibration of the O-H groups of the absorbed water molecules. Furthermore, a distinct sharp band at 471 cm^{-1} was observed for Zn-O bond vibrations (Abdel Aziz et al. 2022).

In the FTIR spectrum of CMC, a broad band of O-H stretching was observed at approximately 3400 cm^{-1}. Symmetric and asymmetric stretching vibrations of the aliphatic C-H bonds were identified at 2880 cm^{-1} and 2921 cm^{-1}, respectively. Additionally, the presence of carboxylate groups was confirmed by the presence of two bands at 1612 cm^{-1} and 1415 cm^{-1}, which were attributed to their asymmetric and symmetric stretching vibrations, respectively, (Salama et al. 2020).

The FTIR of xanthan revealed distinctive bands associated with its structure. The carbonyl stretching of acetyl groups was observed at 1728 cm^{-1}. Moreover, asymmetrical and symmetrical stretching vibrations of the carboxylate groups in the pyruvate and glucuronic acid groups were detected at 1633 cm^{-1} and 1444 cm^{-1}, respectively. The glycosidic bonds of xanthan rings, including –C–O–C–, –C–O–, and –C–C–, were characterized by the absorption bands observed in the range of 1025–1210 cm^{-1} (Cetin et al. 2004; Hamcerencu et al. 2007).

As shown in Fig. 2, some changes were observed in the spectrum of the CMC/Xa film when compared with those of CMC and Xa (Fig. 1). The O–H band became less intense, broadened, and shifted to a lower wavenumber (3240 cm^{-1}) due to the interactions established through hydrogen bonding between CMC and Xa. In addition, the two bands of the asymmetric and symmetric stretching vibrations of COO^- were slightly shifted to lower wavenumbers. These changes between the spectrum of CMC/Xa compared with those of both CMC and Xa confirm the interactions between CMC and Xa in their composite system (CMC/Xa).

The spectrum of CMC/Xa/ZnO-NP films (Fig. 2) exhibited some changes compared to the neat film (CMC/Xa). The O–H vibration band broadened and shifted to 3210 cm^{-1}. In addition, the symmetric and asymmetric stretching vibrations of the carboxylate groups shifted to 1398 cm^{-1} and 1569 cm^{-1}, respectively. These shifts toward lower wavenumbers confirmed the hydrogen bonding between the oxygen atoms of the ZnO-NPs and the hydroxyl and carboxylate groups of CMC and Xa. Additionally, an increase in the ZnO-NPs content resulted in a heightened intensity of a newly observed band at 471 cm^{-1}, corresponding to Zn-O stretching. Based on these changes, it was concluded that the ZnO-NPs were successfully incorporated into the CMC/Xa coating.

XRD

Utilization of the XRD technique yields insights into the crystal structure and dimensions of the crystallites. Fig. 3 shows the XRD patterns of ZnO-NPs, CMC, and Xa, whereas Fig. 5 shows the XRD patterns of CMC/Xa and CMC/Xa/ZnO-NP nanocomposites. The XRD pattern of ZnO-NPs showed sharp characteristic diffraction peaks at 2θ of 31.5° (100), 34.3° (002), 36.2° (101), 47.6° (102), 56.4° (110), 62.6° (103), 67.8° (200) and 69.3° (112) (Li et al. 2008). The average crystallite sizes of ZnO-NPs derived from the Scherrer, W-H, and H-W models (Fig. 4) were 10.19 nm, 10.12 nm, and 11.35 nm, respectively.

Figure 3 demonstrated the amorphous nature of Xa and CMC where broad peaks were observed at 2θ=19.3° (Kwon et al. 2023) and 20.5° (Salama et al. 2020), respectively. The XRD pattern of CMC/Xa showed one broad peak at approximately 2θ=18.7°, suggesting the amorphous nature of the composite, thus confirming the miscibility between CMC and Xa.

Figure 5 illustrates the impact of ZnO-NPs on the crystalline structure of CMC/Xa. The XRD pattern of

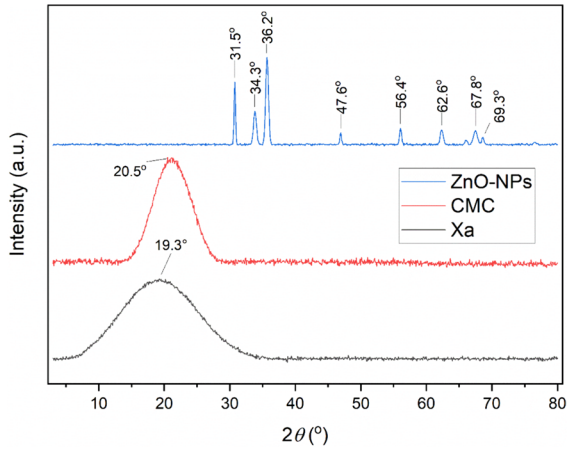


Fig. 3 XRD patterns of ZnO-NPs, CMC, and xanthan

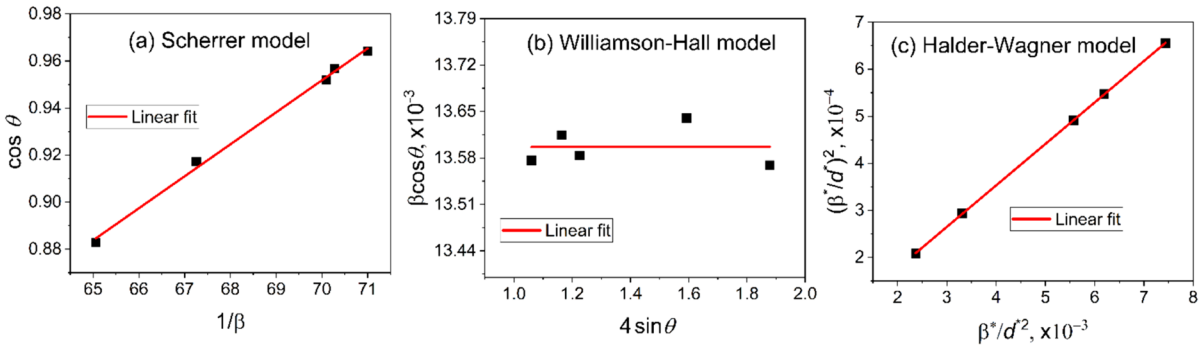


Fig. 4 **a** Scherrer, **b** Williamson-Hall and **c** Halder-Wagner plots

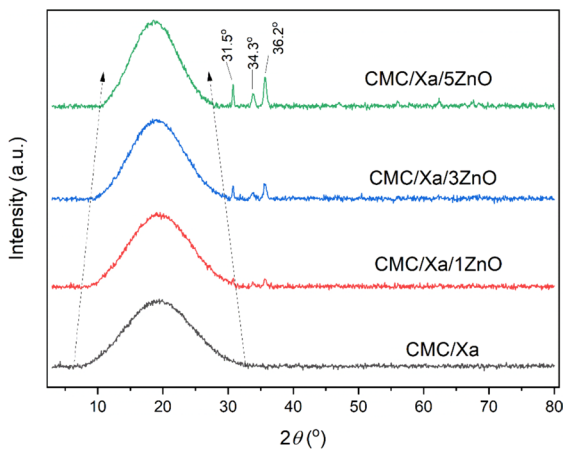


Fig. 5 XRD patterns of CMC/Xa and CMC/Xa/ZnO-NP nanocomposites

the nanocomposites revealed that the intensity of the CMC/Xa peak gradually increased as the content of ZnO-NPs increased. Moreover, at high levels of ZnO-NPs, some distinct sharp peaks of ZnO-NPs [31.5° (100), 34.3° (002), and 36.2° (101)] became visible. These changes provide evidence for the incorporation of ZnO-NPs and their interactions with CMC/Xa polymers.

TEM and DLS

The nanostructured characteristics of the prepared ZnO-NPs were validated through the TEM technique. The TEM image in Fig. 6a shows the presence of uniform and non-agglomerated ZnO-NPs. The average size of ZnO-NPs, determined from the size distribution graph (Fig. 6b), was 13.22 ± 5.11 nm. The size determined by TEM was found to be larger than that estimated using the XRD technique through the Scherrer, W-H, and H-W models. This is because the XRD technique measures the average size of crystallites that combine to form a nanoparticle, and does not account for the hydration of nanoparticles occurred during TEM processing. Additionally, a large size of ZnO-NPs

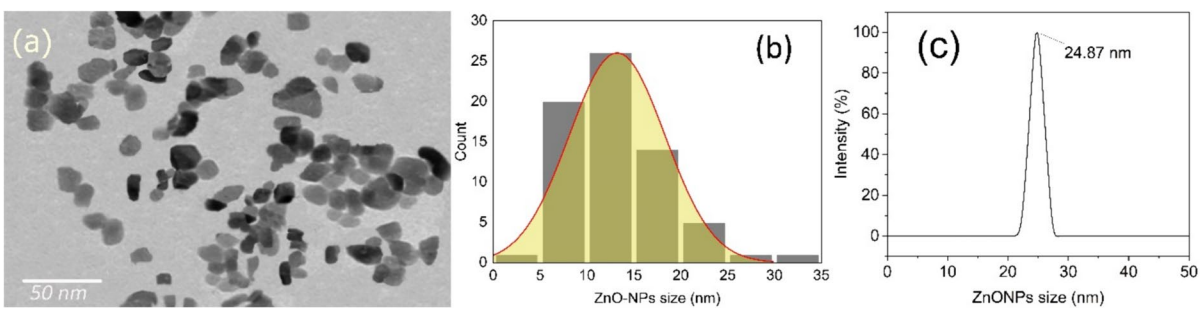


Fig. 6 **a** TEM, **b** the size distribution, and **c** DLS of the prepared ZnO-NPs

Table 1. Thermal parameters and opacity of ZnO-NPs, Xa, CMC, CMC/Xa, and CMC/Xa/ZnO-NP films

Sample	Thermal parameters			Opacity
	IPDT	Char (%)	T_m(°C)	
ZnO-NPs	6877	80.02	309.9	–
Xa	803	30.53	286.7	0.83 ± 0.02^a
CMC	1015	38.95	295.7	0.81 ± 0.02^a
CMC/Xa	901	34.74	292.2	0.92 ± 0.03^a
CMC/Xa/1ZnO	1055	44.17	304.1	1.57 ± 0.05^b
CMC/Xa/3ZnO	1238	49.68	311.3	2.34 ± 0.07^c
CMC/Xa/5ZnO	1447	54.94	320.5	3.02 ± 0.09^d

Means that do not share a letter are significantly different.

(24.87 nm) was obtained using DLS (Fig. 6c). This was attributed to the impact of Brownian motion (Zhang et al. 2016), and the presence of biological materials (CS extract) attached to the surface of the ZnO-NPs (El-Sayed et al. 2021).

TGA

During storage, edible coatings must maintain high thermal stability to prevent thermal decomposition. Table 1 lists the thermal parameters of CMC, Xa, ZnO-NPs, and their composite systems, extracted from their TGA thermograms (Fig. 7, 8). The first stage which occurred around 100°C for all samples, was attributed to water evaporation. As observed in Fig. 7, ZnO-NPs underwent a second stage of mass loss, with a maximum decomposition temperature (T_m) of 309.9 °C. ZnO-NPs also demonstrated a char percentage of 80.02% and a high IPDT of 6877, indicating their outstanding resistance to thermal degradation. Xa and CMC showed a second stage in their decomposition with T_m values of 286.7 °C and 295.7 °C, respectively. This stage was attributed to the breakdown of the primary polymer backbone, which involved decarboxylation, dehydration, and dehydroxylation (Abdel Aziz et al. 2021; Salama et al. 2021).

Fig. 8 and Table 1 illustrate that the composite film CMC/Xa experienced significant decomposition at

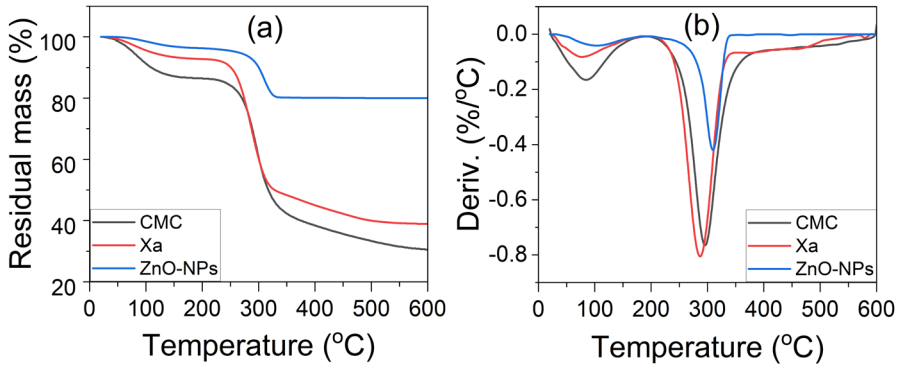


Fig. 7 **a** TGA and **b** DTG of CMC, Xa and ZnO-NPs

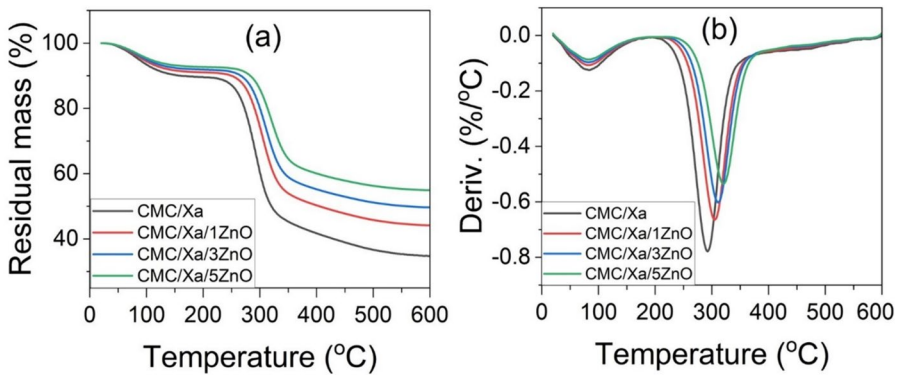


Fig. 8 **a** TGA and **b** DTG of CMC/Xa and CMC/Xa/ZnO-NP films

292.2°C, with IPDT and char values of 901 and 34.74 %, respectively. It was also observed that the thermal stability of the CMC/Xa film was improved after the addition of ZnO-NPs. This was evidenced by the high values of IPDT, and the shift in T_m to higher temperatures, as shown in Fig. 8 and Table 1. This improved stability could be attributed to the thermal insulation provided by the ZnO-NPs. In addition, ZnO-NPs hindered the mass transport of volatile substances generated during thermal degradation. These observations are in agreement with those of previously published reports (Abdel Aziz et al. 2022; Salama et al. 2020). Additionally, as observed from Fig. 8 and Table 1, the notable increase in char content upon the introduction of ZnO-NPs reaffirmed the enhanced resistance to thermal degradation in the presence of ZnO-NPs.

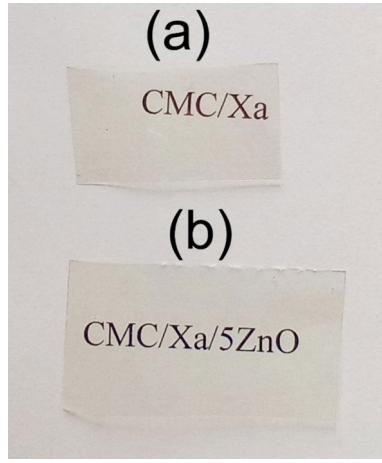


Fig. 9 Photographic images of **a** CMC/Xa and **b** CMC/Xa/5ZnO films illustrating their transparency

Opacity and transparency

Transparent food packaging materials are preferred by consumers; however, for optimal light barrier properties, these materials should be opaque. As shown in Table 1, CMC and Xa films had opacity values of 0.81±0.02 and 0.83±0.02, respectively. In comparison to Xa and CMC, a slight and insignificant rise in the transparency of the composite film (CMC/Xa) was noted at 0.92±0.03. This was ascribed to the interactions between CMC and Xa. As indicated in the introduction of ZnO-NPs led to an increase in the opacity of the CMC/Xa film, reaching 3.02±0.09 when ZnO-NPs were incorporated at 5 wt%. This increased opacity was attributed to light-scattering effect of ZnO-NPs. Similarly, previous studies have reported that ZnO-NPs increased the opacity of alginate/*Citronella oil* (Motelica et al. 2021) and chitosan/*Melissa officinalis* oil films (Sani et al. 2019). Fig. 9 illustrates that the transparency of the CMC/Xa film was not significantly impacted by the incorporation of ZnO-NPs at the highest concentration (5 wt%).

Water vapor permeability (WVP)

WVP measurement assesses the efficacy of edible coatings in inhibiting the transfer of moisture between food and its surroundings. As seen in Table 2, the CMC/Xa film possessed a WVP of 16.2±0.47 g mm/m^2 day kPa which was significantly decreased ($p<0.05$) upon the incorporation of ZnO-NPs. This decrease was attributed to the establishment of hydrogen bonds between the ZnO-NPs and constituents of the CMC/Xa film. Additionally, ZnO-NPs occupy voids within the film structure, impeding the flow of fluids to external environment. Similar effects of ZnO-NPs have been observed in other biopolymer films, such as carrageenan (Meindrawan et al. 2018) and CMC/chitosan films (Noshirvani et al. 2017). These findings indicated that the incorporation of ZnO-NPs improved the fluid barrier properties of CMC/Xa films.

Mechanical properties

The need for edible coatings with enhanced mechanical properties is crucial during the transportation and storage of food products to ensure that they can withstand various physical stresses. The strength and flexibility of coating systems are typically expressed through their tensile strength (TS) and elongation at break (EB), respectively. As shown in Table 2, the CMC/Xa film exhibited TS and EB values of 14.3±0.41 MPa and 32.29±0.93%, respectively. The incorporation of ZnO-NPs into the CMC/Xa film led to a significant increase in TS, reaching 24.07±0.69 at 5 wt% incorporation. This increase in film strength was due to the effective interactions between the ZnO-NPs and the polymer chains in the film. These

Table 2 WVP and mechanical properties of CMC/Xa and CMC/Xa/ZnO-NP films

Sample	WVP (g mm/m^2 day kPa)	Mechanical properties	
		TS (MPa)	EB (%)
CMC/Xa	16.2 ± 0.47^a	14.3 ± 0.41^a	32.29 ± 0.93^a
CMC/Xa/1ZnO	12.57 ± 0.36^b	18.88 ± 0.55^b	29.06 ± 0.84^b
CMC/Xa/3ZnO	8.18 ± 0.24^c	23.12 ± 0.67^c	27.12 ± 0.79^c
CMC/Xa/5ZnO	5.1 ± 0.15^d	24.07 ± 0.69^d	24.22 ± 0.61^d

Means that do not share a letter are significantly different.

findings are consistent with previous reports on the impact of ZnO-NPs on various coating systems such as CMC (Guo et al. 2020), chitosan (Yadav et al. 2021), and olive flounder bone gelatin (Beak et al. 2017).

The addition of ZnO-NPs resulted in a decrease in the EB of the films, suggesting a decrease in their flexibility. The EB was significantly decreased from 32.29±0.93% for CMC/Xa (control) to 24.22±0.61% after the incorporation of ZnO-NPs at 5 wt%. This reduction was attributed to the limited chain mobility caused by the crosslinking interactions facilitated by the presence of ZnO-NPs. Furthermore, the toughness of the films increased in the presence of ZnO-NPs. These observations are consistent with those of previous reports on the effect of ZnO-NPs on agar and carrageenan (Kanmani et al. 2014), chitosan/sodium alginate (Wang et al. 2019), and CMC (Guo et al. 2020).

Antimicrobial properties

Table 3 shows the antimicrobial effects of the coatings on *B. subtilis*, *E. coli*, and *S. racemosum*. No apparent antimicrobial activity was observed for CMC, Xa, and CMC/Xa films against the tested microorganisms. These findings are consistent with those of previous reports (Abdel Aziz et al. 2022; Meydanju et al. 2022; Salama et al. 2020). However, the incorporation of ZnO-NPs into CMC/Xa resulted in significant microbial inhibition. These superior antimicrobial activities of the CMC/Xa/ZnO-NP coatings in comparison to those of the plain CMC/Xa coating could be attributed to the potent antimicrobial properties of ZnO-NPs. The exceptional antimicrobial effects of ZnO-NPs are attributed to the release of Zn^{2+} ions from the nanoparticles. These ions can penetrate the cell membranes of microorganisms and interfere with their negatively charged components, ultimately leading to cell death. Moreover,

Table 3 Bacterial and fungal inhibition zones (mm) of Xa, CMC, CMC/Xa, and CMC/Xa/ZnO-NPs films

Sample	G+ Bacteria *B. subtilis*	G- Bacteria *E. coli*	Fungi *S. racemosum*
Xa	0^a	0^a	0^a
CMC	0^a	0^a	0^a
CMC/Xa	0^a	0^a	0^a
CMC/Xa/1ZnO	15.18±0.44^b	9.21±0.27^b	8.87±0.26^b
CMC/Xa/3ZnO	23.87±0.69^c	11.45±0.33^c	11.87±0.34^c
CMC/Xa/5ZnO	28.62±0.83^d	15.36±0.44^d	14.99±0.43^d
Ampicillin	32.4± 0.3	–	–
Gentamicin	–	17.3±0.1	–
Amphotericin B	–	–	19.7± 0.2

Means that do not share a letter are significantly different.

reactive oxygen species (ROs) produced by ZnO-NPs interact with microorganisms and impair their cell membranes. This effect is attributed to the strong oxidizing effect of these ROs (Krishnamoorthy et al. 2022; Lakshmi Prasanna et al. 2015).

Shelf-life studies

Comparable-sized tomatoes were coated with the CMC/Xa/3ZnO coating using the dipping method to assess its efficacy in extending the shelf life of the food. The CMC/Xa/3ZnO system was selected for testing the coating efficiency because of its excellent properties compared to other systems. Fresh tomatoes without any coating, in addition to tomatoes coated with CMC/Xa and those coated with CMC/Xa/3ZnO, were evaluated for comparison purposes.

Surface spoilage

In Fig. 10, images of tomatoes (coated and uncoated) were captured at selected intervals throughout a 20-day storage period. The images showed that no

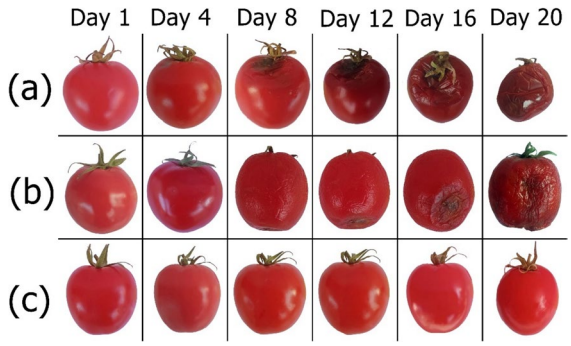


Fig. 10 Surface examination of tomatoes for **a** uncoated, **b** coated with CMC/Xa, and **c** coated with CMC/Xa/3ZnO during storage

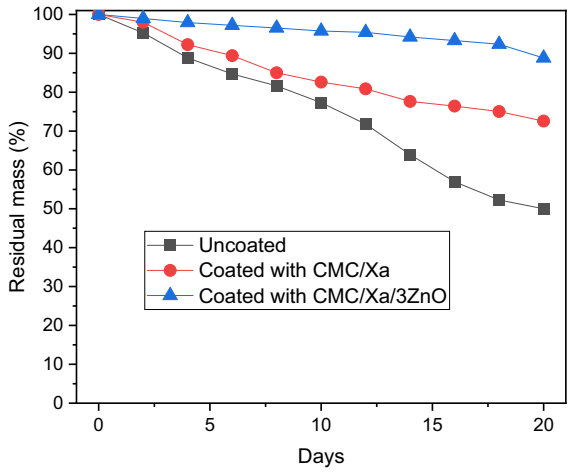


Fig. 11 Mass loss percent of tomatoes during the 20-day storage period

spoilage was detected in tomatoes coated with CMC/Xa/3ZnO throughout the storage period. However, surface spoilage started around the 8th storage day for the uncoated tomatoes and for those coated with the CMC/Xa system. The significant spoilage resistance of tomatoes coated with CMC/Xa/3ZnO returned to the potent antimicrobial characteristics of ZnO-NPs.

Mass loss studies

Edible coatings need to possess a reduced WVP to prevent fluids from leaking from food to its environment. The efficacy of the CMC/Xa/3ZnO coating in retarding fluids leakage from tomatoes over 20 days was demonstrated in Fig. 11. A mass loss of only 11.2% was noted on the 20th day of storage. This was returned to the superior barrier properties of the CMC/Xa/3ZnO coating, which retained fluids inside the coated tomatoes. Conversely, Fig. 11 reveals also that the uncoated tomatoes exhibited a significant mass loss during the storage period, with a mass loss of approximately 50.3% on the 20th day. Additionally, the CMC/Xa-coated tomatoes showed a mass loss of approximately 27.5% on the 20th day due to the poor barrier properties of CMC/Xa coating, resulting in fluid loss to the surrounding environment.

Conclusions

A novel edible coating was developed by incorporating environmentally synthesized ZnO-NPs into the CMC/Xa composite system. FTIR confirmed the successful preparation of ZnO-NPs, and the interactions between the incorporated ZnO-NPs and the components of CMC/Xa system. The nanostructured nature of ZnO-NPs was verified through various techniques: TEM (13.22 ± 5.11 nm), DLS (24.87 nm), XRD (Scherrer (10.19 nm), W-H (10.12 nm), and H-W (11.35 nm)). The thermal stability of coatings was significantly improved upon the incorporation of ZnO-NPs, where the IPDT increased from 901 for CMC/Xa to 1447 for CMC/Xa/5ZnO. The barrier properties of CMC/Xa coating were enhanced as detected from the reduction of WVP from 16.2±0.47 (for CMC/Xa) to 5.1±0.15 g mm/m^2 day kPa when ZnO-NPs were incorporated at 5 wt%. Coatings incorporated with ZnO-NPs maintained sufficient transparency despite the increased opacity in the presence of ZnO-NPs. The inclusion of ZnO-NPs enhanced the strength of the CMC/Xa coating, while reducing its elongation at break. Although the CMC/Xa coating did not inhibit the tested microorganisms, the CMC/Xa/ZnO-NP coatings exhibited significant microbial inhibition. The resulting CMC/Xa/ZnO-NP coatings demonstrated outstanding efficiency in preserving tomatoes against spoilage and significant mass loss for 20 days. The developed CMC/Xa/ZnO-NP coatings showed great potential as viable substitutes for conventional food packaging materials in food packaging industries.

Authors' contributions Hend E. Salama Conceptualization, Data curation, Formal analysis, Investigation, Methodology, Resources, Software, Validation, Writing – original draft, Writing – review & editing. Magdy W. Sabaa Writing – original draft, Writing – review & editing. Mohamed S. Abdel Aziz Conceptualization, Data curation, Formal analysis, Investigation, Methodology, Resources, Software, Validation, Writing – original draft, Writing – review & editing. Maher Khattab Data collection and methodology.

Funding Open access funding provided by The Science, Technology & Innovation Funding Authority (STDF) in cooperation with The Egyptian Knowledge Bank (EKB). Not applicable.

Data availability Data will be available on request.

Declarations

Conflict of interest The authors declare that they have no conflict of interest.

Consent of publication The publication has been approved by all authors.

Ethical approval The authors declare the research did not involve either human participation or animal testing.

Open Access This article is licensed under a Creative Commons Attribution 4.0 International License, which permits use, sharing, adaptation, distribution and reproduction in any medium or format, as long as you give appropriate credit to the original author(s) and the source, provide a link to the Creative Commons licence, and indicate if changes were made. The images or other third party material in this article are included in the article's Creative Commons licence, unless indicated otherwise in a credit line to the material. If material is not included in the article's Creative Commons licence and your intended use is not permitted by statutory regulation or exceeds the permitted use, you will need to obtain permission directly from the copyright holder. To view a copy of this licence, visit http://creativecommons.org/licenses/by/4.0/.

References

Abdel Aziz MS, Salama HE (2021) Developing multifunctional edible coatings based on alginate for active food packaging. Int J Biol Macromol 190:837–844. https://doi.org/10.1016/j.ijbiomac.2021.09.031

Abdel Aziz MS, Salama HE (2022) Development of alginate-based edible coatings of optimized UV-barrier properties by response surface methodology for food packaging applications. Int J Biol Macromol 212:294–302. https://doi.org/10.1016/j.ijbiomac.2022.05.107

Abdel Aziz MS, Salama HE, Sabaa MW (2018) Biobased alginate/castor oil edible films for active food packaging. LWT 96:455–460. https://doi.org/10.1016/j.lwt.2018.05.049

ASTM, E., 96/96M-05 (2005) Standard test methods for water vapor transmission of materials. In. West Conshohocken, PA

Azhdari S, Moradi M (2022) Application of antimicrobial coating based on carboxymethyl cellulose and natamycin in active packaging of cheese. Int J Biol Macromol 209:2042–2049. https://doi.org/10.1016/j.ijbiomac.2022.04.185

Banerjee S, Kaity S. (2019). Pharmaceutical applications of xanthan gum. In *Natural polymers for pharmaceutical applications* (pp. 165-191): Apple Academic Press.

Beak S, Kim H, Song KB (2017) Characterization of an olive flounder bone gelatin-zinc oxide nanocomposite film and evaluation of its potential application in spinach packaging. J Food Sci 82(11):2643–2649. https://doi.org/10.1111/1750-3841.13949

Cetin S, Erdincler A (2004) The role of carbohydrate and protein parts of extracellular polymeric substances on the dewaterability of biological sludges. Water Sci Technol 50(9):49–56. https://doi.org/10.2166/wst.2004.0532

Chaturvedi S, Kulshrestha S, Bhardwaj K, Jangir R (2021) A review on properties and applications of xanthan gum. Applications and Ecological Perspectives, Microbial Polymers. https://doi.org/10.1007/978-981-16-0045-6_4

Ćirić A, Medarević Đ, Čalija B, Dobričić V, Rmandić M, Barudžija T, Malenović A, Djekic L (2021) Effect of ibuprofen entrapment procedure on physicochemical and controlled drug release performances of chitosan/xanthan gum polyelectrolyte complexes. Int J Biol Macromol 167:547–558. https://doi.org/10.1016/j.ijbiomac.2020.11.201

Doyle CD (1961) Estimating thermal stability of experimental polymers by empirical thermogravimetric analysis. Anal Chem 33(1):77–79. https://doi.org/10.1021/ac60169a022

El-Sayed HS, El-Sayed SM, Youssef AM (2021) Novel approach for biosynthesizing of zinc oxide nanoparticles using lactobacillus gasseri and their influence on microbiological, chemical, sensory properties of integrated yogurt. Food Chem 365:130513. https://doi.org/10.1016/j.foodchem.2021.130513

Fan Y, Yang J, Duan A, Li X (2021) Pectin/sodium alginate/xanthan gum edible composite films as the fresh-cut package. Int J Biol Macromol 181:1003–1009. https://doi.org/10.1016/j.ijbiomac.2021.04.111

Guo X, Chen B, Wu X, Li J, Sun Q (2020) Utilization of cinnamaldehyde and zinc oxide nanoparticles in a carboxymethylcellulose-based composite coating to improve the postharvest quality of cherry tomatoes. Int J Biol Macromol. 160:175–182. https://doi.org/10.1016/j.ijbiomac.2020.05.201

Hamcerencu M, Desbrieres J, Popa M, Khoukh A, Riess G (2007) New unsaturated derivatives of xanthan gum: Synthesis and characterization. Polymer 48(7):1921–1929. https://doi.org/10.1016/j.polymer.2007.01.048

Hayta M, Dogan M, Aslan Türker D (2020) Rheology and microstructure of galactomannan–xanthan gum systems at different pH values. J Food Process Eng 43(12):e13573. https://doi.org/10.1111/jfpe.13573

International ASTM (2013) Standard test method for tensile properties of thin plastic sheeting 1. Am Soc Test Mater 14:1–12. https://doi.org/10.1520/D0882-12

Joshy KS, Jose J, Li T, Thomas M, Shankregowda AM, Sreekumaran S, Kalarikkal N, Thomas S (2020) Application of novel zinc oxide reinforced xanthan gum hybrid system for edible coatings. Int J Biol Macromol 151:806–813. https://doi.org/10.1016/j.ijbiomac.2020.02.085

Kanmani P, Rhim JW (2014) Properties and characterization of bionanocomposite films prepared with various biopolymers and ZnO nanoparticles. Carbohydr Polym. 106:190–199. https://doi.org/10.1016/j.carbpol.2014.02.007

Krishnamoorthy R, Athinarayanan J, Periyasamy VS, Alshuniaber MA, Alshammari G, Hakeem MJ, Ahmed MA, Alshatwi AA (2022) Antibacterial Mechanisms of Zinc Oxide Nanoparticle against Bacterial Food Pathogens Resistant to Beta-Lactam Antibiotics. Molecules. 27(8):2489. https://doi.org/10.3390/molecules27082489

Kwon YM, ChangI ChoGC (2023) Xanthan biopolymer-based soil treatment effect on kaolinite clay fabric and structure using XRD analysis. Sci Rep 13(1):11666

Lakshmi Prasanna V, Vijayaraghavan R (2015) Insight into the mechanism of antibacterial activity of ZnO: surface defects mediated reactive oxygen species even in the dark. Langmuir 31(33):9155–9162. https://doi.org/10.1021/acs.langmuir.5b02266

Li C, Li Y, Luo L, Fu M (2008) Synthesis and characterization of ZnO microcrystal tubes. J Chil Chem Soc 53(3):1615–1616. https://doi.org/10.4067/S0717-97072008000300014

Li X, Ren Z, Wang R, Liu L, Zhang J, Ma F, Khan MZH, Zhao D, Liu X (2021) Characterization and antibacterial activity of edible films based on carboxymethyl cellulose, dioscorea opposita mucilage, glycerol and ZnO nanoparticles. Food Chem 349:129208. https://doi.org/10.1016/j.foodchem.2021.129208

Meindrawan B, Suyatma NE, Wardana AA, Pamela VY (2018) Nanocomposite coating based on carrageenan and ZnO nanoparticles to maintain the storage quality of mango. Food Packaging Shelf Life 18:140–146. https://doi.org/10.1016/j.fpsl.2018.10.006

Meydanju N, Pirsa S, Farzi J (2022) Biodegradable film based on lemon peel powder containing xanthan gum and TiO_2–Ag nanoparticles: Investigation of physicochemical and antibacterial properties. Polym Test 106:107445. https://doi.org/10.1016/j.polymertesting.2021.107445

Miles R, Amyes S (1996) Laboratory control of antimicrobial therapy. Mackie McCartney Practical medical microbiology 14:151–178

Motelica L, Ficai D, Oprea O, Ficai A, Trusca RD, Andronescu E, Holban AM (2021) Biodegradable alginate films with ZnO nanoparticles and citronella essential oil-a novel antimicrobial structure. Pharmaceutics 13(7):1020. https://doi.org/10.3390/pharmaceutics13071020

Naseer M, Aslam U, Khalid B, Chen B (2020) Green route to synthesize zinc oxide nanoparticles using leaf extracts of *Cassia fistula* and *Melia azadarach* and their antibacterial potential. Sci Rep 10(1):9055. https://doi.org/10.1038/s41598-020-65949-3

Noshirvani N, Ghanbarzadeh B, Mokarram RR, Hashemi M (2017) Novel active packaging based on carboxymethyl cellulose-chitosan-ZnO NPs nanocomposite for increasing the shelf life of bread. Food Packaging Shelf Life 11:106–114. https://doi.org/10.1016/j.fpsl.2017.01.010

Nsengiyumva EM, Alexandridis P (2022) Xanthan gum in aqueous solutions: Fundamentals and applications. Int J Biol Macromol 216:583–604. https://doi.org/10.1016/j.ijbiomac.2022.06.189

Ostrowski MP, La Rosa SL, Kunath BJ, Robertson A, Pereira G, Hagen LH, Varghese NJ, Qiu L, Yao T, Flint G (2022) Mechanistic insights into consumption of the food additive xanthan gum by the human gut microbiota. Nat Microbiol 7(4):556–569. https://doi.org/10.1038/s41564-022-01093-0

Petri DF (2015) Xanthan gum: A versatile biopolymer for biomedical and technological applications. J Appl Polym Sci. https://doi.org/10.1002/app.42035

Praseptiangga D, Mufida N, Panatarani C, Joni IM (2021) Enhanced multi functionality of semi-refined iota carrageenan as food packaging material by incorporating SiO_2 and ZnO nanoparticles. Heliyon 7(5):e06963. https://doi.org/10.1016/j.heliyon.2021.e06963

Priyadarshi R, Negi YS (2017) Effect of varying filler concentration on zinc oxide nanoparticle embedded chitosan films as potential food packaging material. J Polym Environ 25:1087–1098. https://doi.org/10.1007/s10924-016-0890-4

Ren Z, Li X, Ma F, Zhang Y, Hu W, Khan MZH, Liu X (2022) Oil-in-water emulsions prepared using high-pressure homogenisation with dioscorea opposita mucilage and food-grade polysaccharides: Guar gum, xanthan gum, and pectin. LWT 162:113468. https://doi.org/10.1016/j.lwt.2022.113468

Salama HE, Abdel Aziz MS (2020) Optimized carboxymethyl cellulose and guanidinylated chitosan enriched with titanium oxide nanoparticles of improved UV-barrier properties for the active packaging of green bell pepper. Int J Biol Macromol 165:1187–1197. https://doi.org/10.1016/j.ijbiomac.2020.09.254

Salama HE, Abdel Aziz MS (2021) Development of active edible coating of alginate and aloe vera enriched with frankincense oil for retarding the senescence of green capsicums. LWT 145:111341. https://doi.org/10.1016/j.lwt.2021.111341

Sani IK, Pirsa S (2019) Preparation of chitosan/zinc oxide/melissa officinalis essential oil nano-composite film and evaluation of physical, mechanical and antimicrobial properties by response surface method. Polym Test 79:106004. https://doi.org/10.1016/j.polymertesting.2019.106004

Sen SK, Barman UC, Manir M, Mondal P, Dutta S, Paul M, Chowdhury M, Hakim M (2020) X-ray peak profile analysis of pure and dy-doped α-MoO_3 nanobelts using debye-scherrer, williamson-hall and halder-wagner methods. Advances in Natural Sciences: Nanoscience and Nanotechnology 11(2):025004. https://doi.org/10.1088/2043-6254/ab8732

Smaoui S, Chérif I, Ben Hlima H, Khan MU, Rebezov M, Thiruvengadam M, Sarkar T, Shariati MA, Lorenzo JM (2023) Zinc oxide nanoparticles in meat packaging: A systematic review of recent literature. Food Packag Shelf Life 36:101045. https://doi.org/10.1016/j.fpsl.2023.101045

Surendra B, Swamy MM, Shamala T, Rao S, Pramila S (2022) Development of enhanced electrochemical sensor and antimicrobial studies of ZnO NPs synthesized using green plant extract. Sens Int 3:100176

Wang H, Gong X, Miao Y, Guo X, Liu C, Fan YY, Zhang J, Niu B, Li W (2019) Preparation and characterization of multilayer films composed of chitosan, sodium alginate and carboxymethyl chitosan-ZnO nanoparticles. Food Chem. 283:397–403. https://doi.org/10.1016/j.foodchem.2019.01.022

Xu W, Jin W, Huang K, Huang L, Lou Y, Li J, Liu X, Li B (2018) Interfacial and emulsion stabilized behavior of lysozyme/xanthan gum nanoparticles. Int J Biol Macromol 117:280–286. https://doi.org/10.1016/j.ijbiomac.2018.05.187

Yadav S, Mehrotra GK, Dutta PK (2021) Chitosan based ZnO nanoparticles loaded gallic-acid films for active food packaging. Food Chem 334:127605. https://doi.org/10.1016/j.foodchem.2020.127605

Yang X, Li A, Li D, Li X, Li P, Sun L, Guo Y (2020) Improved physical properties of konjac glucomannan gels by co-incubating composite konjac glucomannan/xanthan systems under alkaline conditions. Food Hydrocoll 106:105870. https://doi.org/10.1016/j.foodhyd.2020.105870

Zhang XF, Liu ZG, Shen W, Gurunathan S (2016) Silver nanoparticles: Synthesis, characterization, properties, applications, and therapeutic approaches. Int J Mol Sci 17(9):1534. https://doi.org/10.3390/ijms17091534

Publisher's Note Springer Nature remains neutral with regard to jurisdictional claims in published maps and institutional affiliations.